DOI: 10.17617/2.3194856
Proceedings of the 9th Solar Polarization Workshop SPW9
A workshop held in Göttingen, Germany, from August 26 to August 30, 2019
Achim Gandorfer, Andreas Lagg, Kerstin Raab (eds.)

Simulation of high spatial resolution polarimetry with the Chinese Giant Solar Telescope

Shu Yuan[1,*], Yu Fu[1], Igor Di Varano[2], Zhenyu Kim[1], and Zhong Liu[1]

[1]Yunnan Observatories, CAS, Yangfangwang 396, Guandu district, Kunming, China
[2]Leibniz Institute for Astrophysics Potsdam (AIP), An der Sternwarte 16, D-14482 Potsdam, Germany
[*]*Email:* yuanshu@ynao.ac.cn

Abstract. The polarization imaging properties of the Chinese Giant Solar Telescope (CGST) in the case of near-diffraction-limited Imaging Spectro-polarimetry are investigated in this paper, which points towards a conflict between high spatial resolution and high polarimetric accuracy, due to the existence of polarization aberrations. We adopt the method of scientific integrated simulation for this investigation, which combines MHD simulations of small-scale magneto-convection in the photosphere of the Sun with the point spread matrix of the telescope. A polarization simulator tool for reflective telescopes is developed for calculating the Jones pupil at the Coudé focus, which is transformed to the point spread matrix by Fourier optics. For the current optical design, the theoretical instrumental polarization of the Chinese Giant Solar Telescope is negligible, by its polarization-compensated optical configuration in the Coudé trains. But the polarization aberrations, which are caused by right angle reflection at the folding mirrors in a fast beam result in a polarization ghost point spread function, and thus a spurious polarization signal in the Stokes images and the spectral profiles for a given target. The structure of the spurious signal shows the characteristics of high spatial frequencies and is nonuniform over the simulation area. The maximum value of the spurious signal is about 1e-3, which is comparable to the underlying solar signal under investigation.

1 Introduction

The Chinese Giant Solar Telescope is the next generation ground-based large solar telescope plan in China, which is currently designed to be an 8m Ring Solar Telescope (Deng & CGST Group 2011; Liu et al. 2012, 2014), whose conceptual design is shown in figure 1. The primary scientific goal of CGST is to acquire systematic knowledge of the finest magneto-hydrodynamic processes in the lower solar atmosphere. In order to achieve this goal, CGST should be able to accurately measure the vector magnetic field with a spatial scale of 20km (0.028arcsec) and a temporal resolution of sub-second, from the lower photosphere to the higher chromosphere (Liu et al. 2016). The vector magnetic fields in the solar atmosphere cannot be observed directly, but can be diagnosed from the imprints of the Zeeman effect on its polarized spectral line profiles (Stokes profiles). In some science cases, the magnetic field strength can be as low as 5 Gauss in both, the transverse and the longitudinal direction. Thus

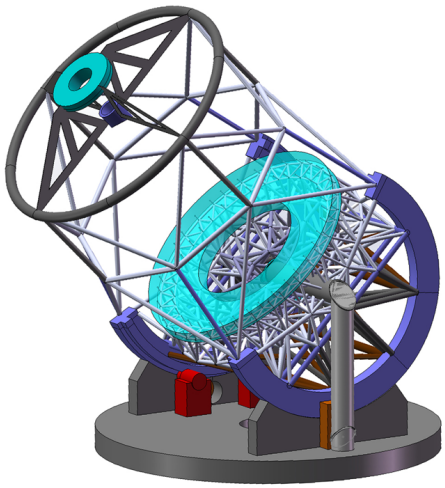

Figure 1. A conceptual design of the Chinese Giant Solar Telescope

CGST must be able to detect solar polarization with an accuracy down to 2e-4. On the other hand, the diffraction-limited resolution of an 8 m aperture telescope in the visible is about 15km. So the observation of near-diffraction-limited spectro-polarimetry or magnetography with high accuracy will be pursued by CGST. In such a case, the vectorial diffraction property of the telescope must be considered.

Vectorial imaging is a kind of physical optical property for polarization-sensitive systems, which means that the image formation of the system is depending not only on the system imaging properties, but is also sensitive to the input polarization state. The physical reason of vectorial imaging in a reflective telescope is polarization aberrations caused by the non-uniformity of the instrumental polarization in the pupil. The effect leads to cross-talk and to spurious polarization in the output polarization images of the telescope. This spurious polarization contains spatial features and therefore cannot be eliminated by either the recent scalar reconstruction method or by polarization calibration of the telescope based on a single Mueller matrix. Thus the polarimetric accuracy of CGST may be impacted by this effect in the case of near-diffraction-limited polarimetry. New design methods of polarization optics and techniques of high-resolution image reconstruction must be adopted in CGST in order to achieve its ultimate spatial resolution and polarimetric accuracy.

The early theory of vectorial imaging was developed by van Weert, according to whom the point spread function of an imaging system is characterized by a tensor function, and the well-known scalar theory and the Jones calculus are both incorporated into this theory (van Weert 1978). The vectorial properties of the telescope are a result of polarization aberrations, describing the distribution of instrumental polarization over the wavefront. McGuire and Chipman derived the formulae of a 4×4 point spread matrix (PSM) and the optical transfer matrix for optical systems with polarization aberrations (McGuire & Chipman 1990, 1991). Almeida and Pillet developed a technique to model the polarimetric point spread function (Sanchez Almeida & Martinez Pillet 1992) and discussed the seeing effects on it. Breckin-

ridge and et. al. discussed the ghost PSF, which is caused by polarization aberrations in a stellar coronagraph (Breckinridge et al. 2015; Breckinridge & Chipman 2016).

In this paper, we develop a numerical method in order to simulate the PSM for an arbitrary optical configuration of a reflecting telescope, and we use the simulated PSM of CGST to discuss the relation between the spatial resolution and the polarimetric accuracy, based on an integrated scientific simulation. This paper is organized as follows: The integral formalism of the PSM is derived in the next section. Section 3 describes the numerical solution of this formula. The simulation results of CGST are discussed in section 4. The scientific integrated simulation (observational simulation) of imaging polarimetry with an artificial target of small-scale magnetoconvection is presented in section 5. A discussion and conclusion will be given in Sect. 6 and 7, respectively.

2 The formula of the point spread matrix

For the case of diffraction-limited polarimetry, the vectorial diffraction properties of the telescope can be characterized by the PSM, which can be regarded as a combination of the scalar point spread function (PSF) with a Mueller matrix, and which defines the linear transformation from the incident polarization state, $\mathbf{I}_{in} = [I, Q, U, V]^T$, to the Stokes impulse response of the telescope $\mathbf{S}$. This relation is written as

$$\mathbf{S}(\mathbf{r}_p, \mathbf{s}_i) = \mathbf{M}(\mathbf{r}_p, \mathbf{s}_i)\mathbf{I}_{in}, \tag{1}$$

where the $\mathbf{r}_p$ represents the spatial variable, and $\mathbf{s}_i$ is the direction vector of the incident plane wave with respect to the optical axis of the telescope. In order to calculate the PSM, the Jones formalism, which contains the phase information, must be used for the diffraction integral, and a counterpart of the Jones formula to the Eq. 1 can be written as

$$\mathbf{E}_t(\mathbf{r}_p, \mathbf{s}_i) = \mathbf{D}_t(\mathbf{r}_p, \mathbf{s}_i)\mathbf{E}_{in}, \tag{2}$$

where $\mathbf{E}_{in}$ is the incident Jones vector, $\mathbf{E}_t$ is the corresponding field distribution in the image plane, and the transfer matrix, $\mathbf{D}_t$, is called the amplitude response matrix (ARM). According to the transformation between the Stokes and the Jones vector, the PSM can be written by the ARM as follows

$$\mathbf{M}(\mathbf{r}_p, \mathbf{s}_i) = \mathbf{B}[\mathbf{D}_t(\mathbf{r}_p, \mathbf{s}_i) \otimes \mathbf{D}_t^*(\mathbf{r}_p, \mathbf{s}_i)]\mathbf{B}^{-1}, \tag{3}$$

where the symbol $\otimes$ indicates the Kronecker product, $*$ represents the conjugate, and the transformation matrix between the Stokes vector and the coherent vector is written as

$$\mathbf{B} = \begin{pmatrix} 1 & 0 & 0 & 1 \\ 1 & 0 & 0 & -1 \\ 0 & 1 & 1 & 0 \\ 0 & j & -j & 0 \end{pmatrix}. \tag{4}$$

For a geometrical optical system, the electromagnetic field propagating through it can be decomposed into a set of plane waves, or light rays, starting from the entrance and going down to the image plane. Thus the image formation can be explained as a coherent superposition of all the rays from the entrance. For a single ray, the Jones vector distribution around its footprint on the image plane can be written as

$$\mathbf{E}(\mathbf{r}_p) = \mathbf{D}(\mathbf{r}_i, \mathbf{s}_i)\mathbf{E}_{in} e^{-jk\left[\phi_{in}+\phi_i+n\mathbf{s}\cdot(\mathbf{r}_p-\mathbf{r}_s)\right]}, \tag{5}$$

where $\mathbf{D}$ is the Jones matrix for a specific ray passing through the system, ϕ_{in} is the eikonal distribution function of the incident light in the entrance, ϕ_i is the eikonal function for the given ray from the entrance to the image plane, $\mathbf{s}$ is the direction vector of the ray close to the image plane, and $\mathbf{r}_s$ is the position of the intersecting ray on the plane. For a given reflective telescope, a specific ray can be defined by $\mathbf{r}_i$, and $\mathbf{s}_i$. So its polarization properties can be calculated by the technique of polarization ray tracing with the optical properties of the coating material on each surface. Based on the Huygens-Fresnel principle, the integral field on the image plane can be written as

$$\mathbf{E}_t(\mathbf{r}_p) = \int_{\Sigma_i} \mathbf{D}(\mathbf{r}_i, \mathbf{s}_i)\mathbf{E}_{in} e^{-jk\left[\phi_{in}+\phi_i+n\mathbf{s}\cdot(\mathbf{r}_p-\mathbf{r}_s)\right]} d\Sigma_i. \tag{6}$$

If we don't consider the wavefront deformation due to atmospheric seeing, $\mathbf{E}_{in}$ is uniform over the whole entrance, and can be removed from from Eq. 6. So, according to Eq. 2, the ARM can be written as

$$\mathbf{D}_t(\mathbf{r}_p, \mathbf{s}_i) = \int_{\Sigma_i} \mathbf{D}(\mathbf{r}_i, \mathbf{s}_i) e^{-jk\left[\phi_{in}+\phi_i+n\mathbf{s}\cdot(\mathbf{r}_p-\mathbf{r}_s)\right]} d\Sigma_i. \tag{7}$$

By Eq. 3 and 7, and by polarization ray tracing, the PSM of a given telescope with a geometric model and a coating prescription can be numerically calculated as follows.

3 The point spread matrix of CGST

3.1 Optical configuration of CGST

Differing from the early narrow ring design, the recent optical configuration of CGST is more moderate, since the ring width has been increased to 2m from the previous 1m. Thus the collecting area of CGST is equivalent to a telescope with a 7m full aperture. The main telescope of CGST is a typical Gregorian system, which is mounted into an altitude-azimuth mechanical structure. The Gregorian focus, located below the primary mirror, is rotationally symmetric. The f-numbers in the primary and secondary focus are 1.57 and 11.3, respectively. After the Gregorian focus, optical trains relay the sunlight down to the Coudé focus, which adopts a polarization-compensated geometry in order to minimize the instrumental polarization, and which increases the f-number to 45. This design is shown in Figure 2. A more detailed optical layout of the Coudé optics is shown in Figure 3. Here, a pair of orthogonal diagonal mirrors, M3 and M4, feed the light into the horizontal elevation axis of the telescope. The light is then reflected backwards to another pair of folding mirrors, M6 and M7, via the relay mirror M5. Thanks to the orthogonality of the incidence plane between the two sequential diagonal mirrors, both, their attenuation and their retardance compensate each other for a paraxial ray. Thus in principle, each of the diagonal mirror units is 'polarization free'. When the elevation changes, M4 and M3 will rotate about the altitude axis together, and the polarization compensation of these trains is not broken. On the other hand, it should be noted that the symmetry axis of the main telescope, the altitude axis and the azimuth axis do not intersect with each other in space.

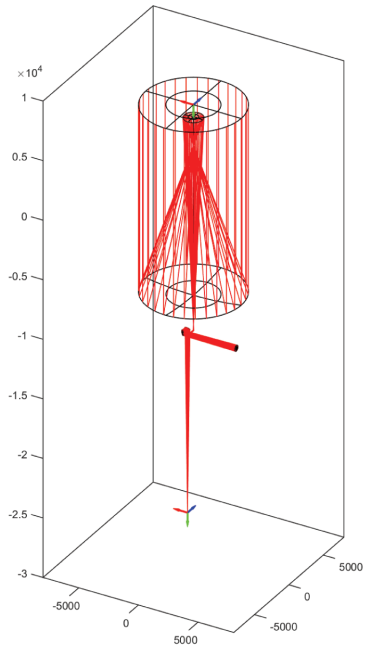

Figure 2. Recent optical configuration of CGST

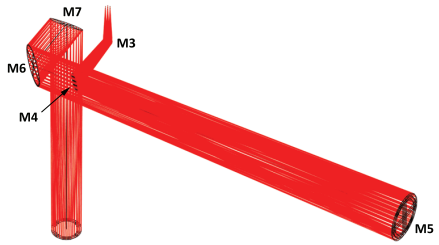

Figure 3. Local optical layout of the Coudé trains

3.2 Polarization ray-tracing

For the calculation of the Jones matrix **D** in Eq. 7, an algorithm of polarization ray-tracing based on Jones formulae has been developed, which is achieved by the technique of integrated modeling. This model uses the commercial software Zemax to calculate the geometry for each ray, and Matlab to calculate the polarization transfer properties for each optical surface. The two software packages communicate with each other by dynamic data exchange (DDE), where Zemax plays the role of the server and Matlab as client. In our algorithm, the client requests the section coordinates on each optical surface for a specific ray defined in Matlab. Then the retrieved coordinates are used for calculating the incidence angle of each surface

Table 1. Optical properties of the coating materials

Line	λ(nm)	aluminum	silver
Fe I	532.4	$0.9405 + i\,6.4242$	$0.0542 + i\,3.4328$
Fe I	630.1	$1.4303 + i\,7.5081$	$0.0569 + i\,4.2543$
He I	1083	$1.3618 + i\,10.463$	$0.0400 + i\,7.7560$
Fe I	1565	$1.6017 + i\,15.816$	$0.1459 + i\,11.487$

and the rotation angle of the coordinate frame between successive planes of incidence. The incidence angles are used for calculating the transformation matrix of a reflection by the polarization model of the coating, and the rotation angle is used for the coordinate transformation of the polarization state between successive surfaces. Finally, the total matrix for a specific ray is calculated by multiplying these above mentioned matrices in the order of propagation, with the user-defined input and output coordinate system.

3.3 Polarization model of metallic coating

In polarization ray-tracing, the Jones matrix of a metallic reflection in its eigen-coordinate system can be written as

$$d = \begin{pmatrix} r_s & 0 \\ 0 & r_p \end{pmatrix}, \tag{8}$$

where r_s and r_p are complex amplitudes for the reflectance(AR) of a transverse electric(TE) and a transverse magnetic(TM) wave, respectively. Rigorously, the AR should be calculated by the matrix theory of thin films, due to the multi-layer structure of the actual mirror coating. But, at the moment, we just consider the simplest case of a bare metal coating and thus ignore the effect of the finite thickness of the coating. Thus, the AR can be derived from the Fresnel formulae directly, which is written as follows (Keller 2002)

$$r_s = \frac{\cos i - n\cos r}{\cos i + n\cos r}, \tag{9}$$

$$r_p = \left(\frac{n\cos r - \cos i}{\cos i + n\cos r}\right)\left(\frac{n\cos r\cos i - \sin^2 i}{n\cos r\cos i + \sin^2 i}\right), \tag{10}$$

where n is the complex index of refraction (CIR) of metal, i and r are the complex angles of the incident and refracted light, respectively. By Snell's law, the item of $n\cos r$ can be replaced by $\sqrt{n^2 - \sin^2 i}$, then all the variables in Eq. 9 and 10 are physical. According to the current optical design, the primary mirror of CGST uses a bare aluminum coating, and the secondary mirror uses protected silver, while the other mirrors use aluminum tentatively. Table 1 shows the theoretical CIR of aluminum (Rakic 1995) and silver (Johnson & Christy 1972) for different spectral lines, which are relevant for CGST polarimetry. For the following simulation work, the Fe I 630.2 nm will be used.

3.4 Results of the telescope point spread matrix simulation

Based on the polarization ray-tracing and the polarization model of the coating, the JP of CGST is calculated. Figure 4 displays the PSM simulation result of CGST at the Gregorian

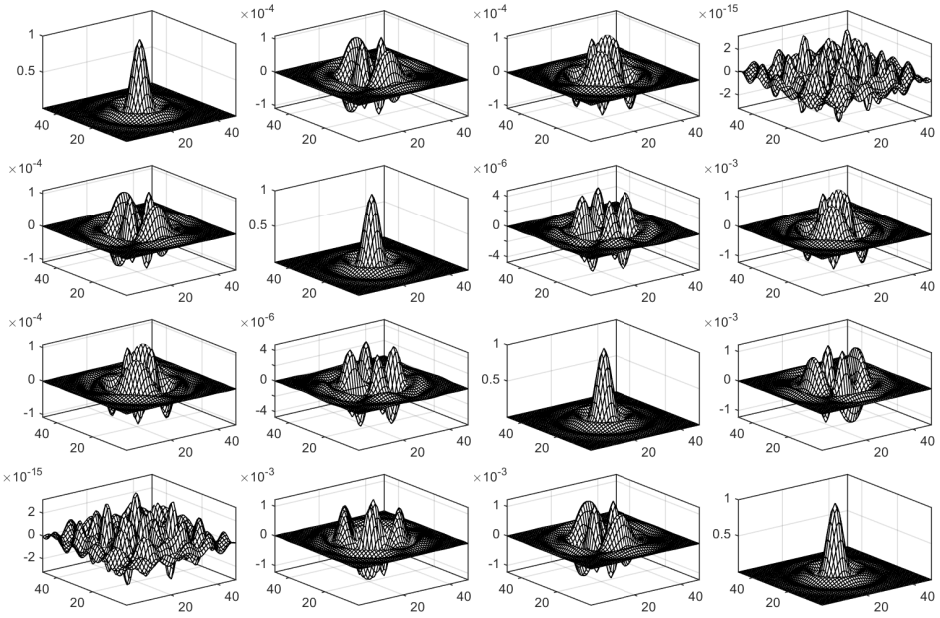

Figure 4. Profiles of the point spread matrix at the Gregorian focus at a wavelength of 632.1nm

focus, which is normalized to the maximum of the first matrix element. The maximum and minimum of each matrix element are shown in each subplot.

Generally, all terms in this PSM express a rotationally functional symmetry, corresponding to the rotational symmetry of the optics before the Gregorian focus. The diagonal terms are dominating in the matrix, and are identical to the Airy disk of the ring aperture. The amplitude of the linear polarization terms are at a level of 1e-4, and the cross-talk terms between Q,U and V are about 1e-3. This PSM indicates that even at a 'polarization-neutral' focus, there is an instrumental polarization effect, with spatial properties and consequences for diffraction-limited polarimetry. In addition, besides the spatial variability, the PSM is also a function of the target position in the field of view (FoV). Figure 5 presents the evolution of the circular polarization at the term of (4,1) from the center of the field-of-view towards the edge, where an anti-symmetric profile is growing gradually form 0 to 3.2e-4.

Figure 6 displays the PSM at the Coudé focus. Compared to the previous one, the last two diagonal terms have an inverted profile due to the odd reflection in the path. At the same time, all non-diagonal terms change from symmetric to anti-symmetric or asymmetric functions, and grow in different degree. This is a result of the multiple reflections by the folding mirrors, which break the rotational symmetry of the optical system. By integrating this PSM in the space domain, we get the net Mueller matrix of the telescope at the Coudé

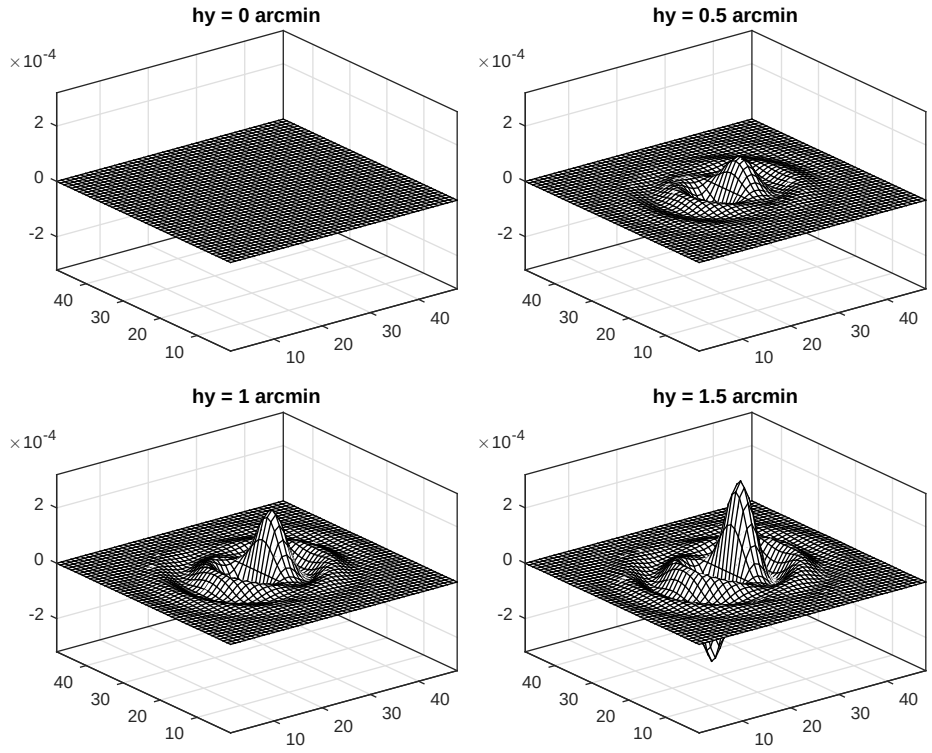

Figure 5. Evolution of the circular polarization (term 4,1) of the PSM from the center to the edge of the field of view, where hy is the object height in arc-minutes

focus such as

$$\mathbf{M}_c = \begin{pmatrix} 1.0000 & 0 & 0 & -0.0001 \\ 0 & 0.9998 & 0.0002 & 0 \\ 0 & 0.0002 & -0.9997 & 0 \\ 0.0001 & 0 & 0 & -0.9997 \end{pmatrix}, \tag{11}$$

which is equivalent to the average of all the Mueller matrices of the ray bundle in the aperture. In Eq. 11, only four non-diagonal elements get to the level of 1e-4, which are cross-talk terms between Q and U, and circular polarization terms. All of them are below the accuracy requirement (2e-4) of CGST. By dividing the PSM of the Coudé focus by $\mathbf{M}_c$, the 'corrected' PSM can be obtained, which is shown in figure 7. In this PSM, the inverted diagonal elements are amended, the asymmetry of the linear cross-talk terms is eliminated by removing the component of diagonal terms in it previously. The largest terms in figure 7 are PSM(2,1), (3,1) and (1,2), (1,3), where the PSM(2,1) and (3,1) mean polarization from I to Q and U, and whose amplitudes are about 9.2e-3 and 6.2e-3, respectively. By these two terms, spurious polarization (SP) caused by the telescope may arise, whose strength does not only depend on the telescope, but also on the spatial and spectral features of the target. Therefore an

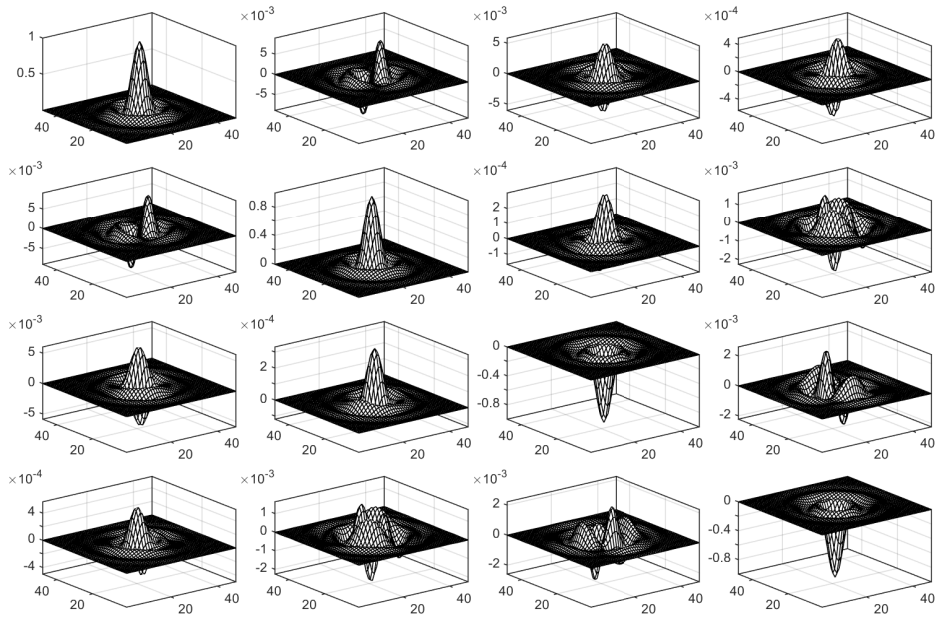

Figure 6. Profiles of the point spread matrix at the Coudé focus without instrumental polarization correction at the wavelength of 630.1nm

integrated scientific simulation with an artificial target became necessary in order to evaluate the performance of the recent design.

4 Scientific integrated simulation

The simulation results of magnetohydrodynamics (MHD) on mesogranular and granular scales on the solar surface by Stein (Stein & Nordlund 2006) are used to investigate the performance of imaging polarimetry, especially the SP caused by the first column of figure 7. Figure 8 displays the original simulated magnetoconvection data from Stein's personal homepage, where the left is the intensity of the continuum in an area of 1008×1008 with 6 km pixels size, and the right is the corresponding vertical magnetic field distribution. By radiative transfer equations, the Stokes profiles of the line of Fe I 6301 is calculated, and 256×256 local Stokes images in the line wing of 6301.44 Åare shown in the first row of figure 9, whose position is marked by the white box in figure 8. Due to the normalization of each Stokes image by the average intensity in the whole simulation domain, the local intensity maybe higher than unity.

Just as for the PSF in a scalar imaging system, the PSM plays the same role as a tensorial filter in a vectorial imaging system. So the output Stokes images of a telescope can be obtained by convolving the input Stokes images with the PSM following the principle of matrix multiplication, whose formulae can be written as Eq. 12.

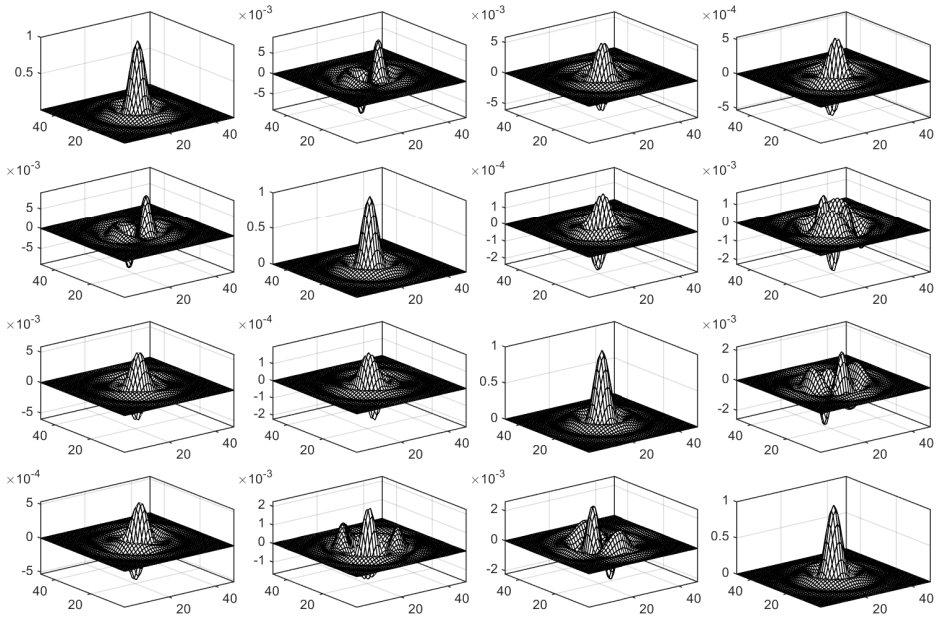

Figure 7. Profiles of the point spread matrix at the Coudé focus with instrumental polarization correction at the wavelength of 630.1nm

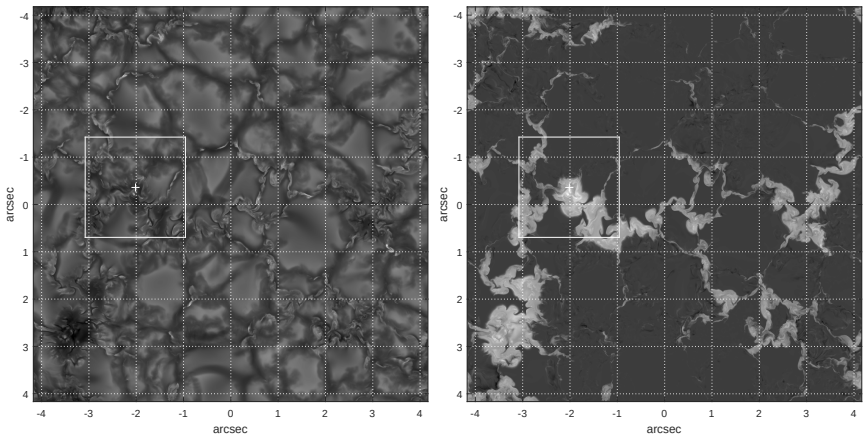

Figure 8. Magnetoconvection simulation: Intensity of the continuum (left) and vertical magnetic field B_z in an optical depth of $\tau = 1$ (right)

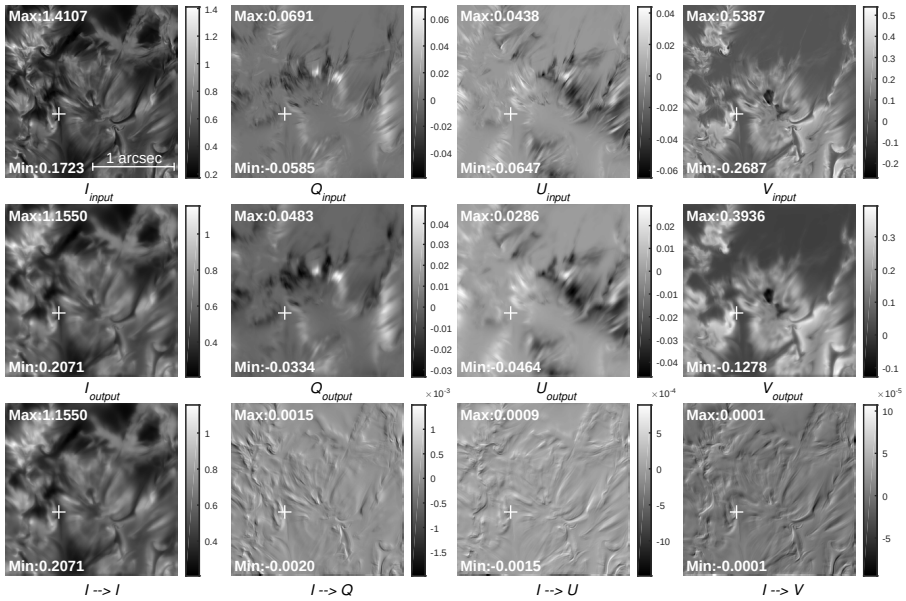

Figure 9. Results of a scientific integrated simulation of diffraction-limited polarimetry of CGST in the line wing

$$\mathbf{S}(x_i, y_i) = \mathbf{M} \otimes \mathbf{I}_{in}(x_0, y_0), \tag{12}$$

where (x_0, y_0) and (x_i, y_i) present the coordinates of the input and the output images, respectively, and $\otimes$ is the convolution symbol. The second row in figure 9 display the output Stokes images of CGST at the Coudé focus by Eq. 12. Generally, when comparing the input and the output Stokes images, there is a low-pass behaviour of the telescope, which is related to the diagonal terms of the PSM in figure 7. The components of the SP in the output images are displayed individually in the third row of figure 9. Obviously, the distribution of the SP is related to the spatial structure of the intensity, with a maximum of about -2e-3 in Stokes Q. Actually, the SP have a feature of gradients of the intensity, due to the anti-symmetric profile of the first column in the PSM. Figure 10 displays the comparison between input and output Stokes profiles at the position marked by the white plus in figure 9. There we notice that the SP in the Stokes profiles of Q and U has remarkable spectral features, which represent a non-zero background in the continuum, but a small smoothing around the line.

5 Discussion

In order to clarify the relation between spatial resolution and polarimetric accuracy empirically, a contour map of the SP of Stokes Q in figure 9 is drawn in figure 11. The green background represents the area whose absolute value is lower than the accuracy requirement (2e-4). The value in the yellow area is larger than this 2e-4, but smaller than 1e-3, and the

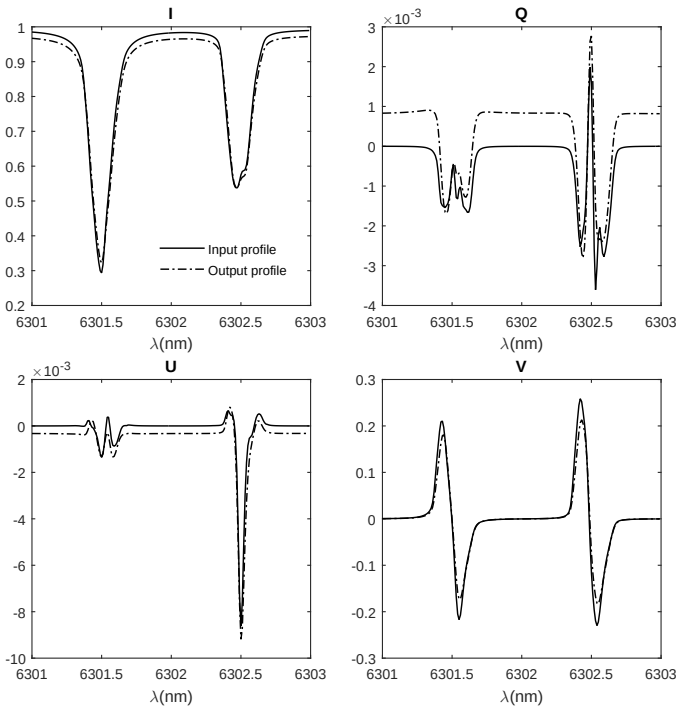

Figure 10. Comparison between input and output Stokes profiles in the diffraction-limited case

blue area is just the reverse. The red and deep blue peaks are areas, in which the absolute value is larger than 1e-3. Obviously, the non-negligible SP in the simulation area are not unique but general. In addition, the structure of strong SP represents the features of high spatial frequency. This feature reveals the conflict between spatial resolution and polarimetric accuracy on a high resolution object. Generally, higher resolution means higher SP, thus lower accuracy. On the contrary, improving the polarimetric accuracy is always at the price of decreasing the spatial resolution, actively or passively.

Based on the above simulations, we could foresee that the SP caused by polarization aberrations of the system will be an important issue in high resolution polarimetry of CGST. So, how to eliminate this effect will be a research subject of polarization optical design and observational method choice for CGST. Currently, there are two strategies for solving this problem. One is to avoid the large angle of oblique reflection in fast beams, which can decrease polarization aberrations, thus improving the vectorial imaging properties of the telescope. But this solution will inevitably increase the size of the folding mirrors and the length of the light path. The other one is to use the model of vectorial imaging of the telescope to reconstruct the original Stokes images from the observational data. In this case, a deconvolution of the PSM from the polarimetric data is necessary. By that time, how to obtain the actual PSM of the telescope will be an important question.

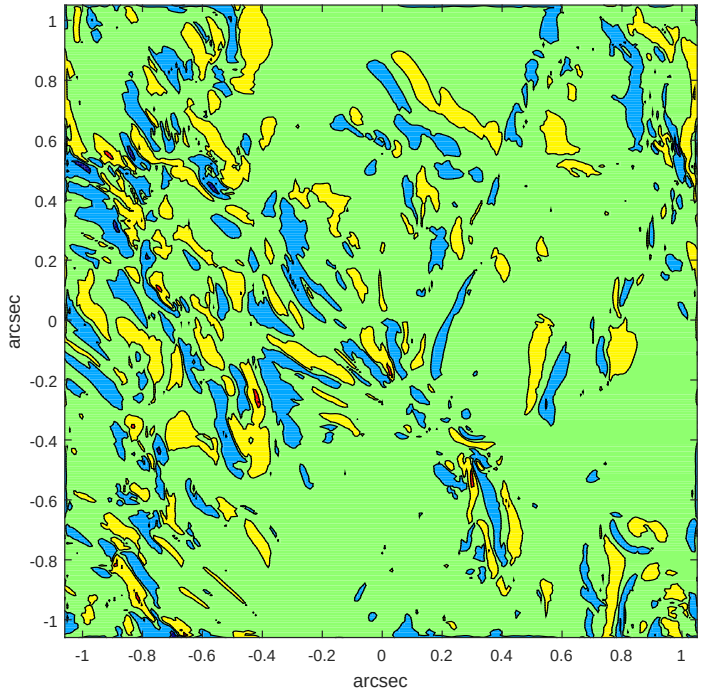

Figure 11. Contour map of spurious signals in Stokes Q at the line wing

6 Conclusions

Near-diffraction-limited polarimetry with high accuracy will be pursued by CGST in order to explore the finest magneto-hydrodynamic processes on the Sun. The aim of the present research is to investigate the relation between spatial resolution and polarimetric accuracy for the recent telescope design, which have revealed a dependency of the vectorial diffraction effect of the telescope. In this paper, the point spread matrix (PSM) was used to characterize this vectorial property, which defines the polarized impulse response of the telescope. Based on the formulae of the vectorial diffraction integral and the technique of polarization ray-tracing, a numerical method has been developed to simulate the PSM for arbitrary symmetric or asymmetric optical configurations. The PSM at the Gregorian and the Coudé focus were simulated, respectively. The profiles in the non-diagonal terms of the PSM at the Gregorian focus is symmetric, and too low to be considered, according to the accuracy requirement of CGST. In this part, the telescope can be assumed safely as a scalar imaging system, because the image formation for each Stokes component is independent of the others. In the PSM of the Coudé focus, an anti-symmetric profile in the non-diagonal terms appears, which is a byproduct of the oblique reflection of the pencil beam in the Coudé trains. In this part, the folding mirrors of M3 and M4 give a dominant contribution of polarization aberrations in the

train due to the small f-number. By convolving the resulting PSM with a simulated target, we obtained the Stokes images at the Coudé focus. The main feature of the output Stokes images is the remarkable component of spurious polarization (SP), which is a function of the intensity image and the spectral profile of the target. The largest SP is 2.3e-3 happening in the line wing of Stokes Q. Due to its high frequency characteristics, it is very hard to separate the SP from the original signal, by the recent scalar image reconstruction. Low-pass filtering of the Stokes image can suppress the SP down to the accuracy requirement, but paying a big price in resolution. It can be predicted that a vectorial image reconstruction technique must be developed in the future, for achieving near-diffraction-limited polarimetry with the desired accuracy.

Acknowledgements. The authors gratefully acknowledges the support of NSFC grants 11773069, K. C. Wong Education Foundation and DAAD. The authors thank Prof. R. F. Stein of Michigan State University for the generous permission to use his MHD simulation data.

References

Breckinridge, J. B. & Chipman, R. A. 2016, in Society of Photo-Optical Instrumentation Engineers (SPIE) Conference Series, Vol. 9904, Space Telescopes and Instrumentation 2016: Optical, Infrared, and Millimeter Wave, 99041C

Breckinridge, J. B., Lam, W. S. T., & Chipman, R. A. 2015, Publications of the Astronomical Society of the Pacific, 127, 445

Deng, Y. Y. & CGST Group. 2011, in Astronomical Society of India Conference Series, Vol. 2, 31–36

Johnson, P. B. & Christy, R. W. 1972, Phys. Rev. B, 6, 4370

Keller, C. U. 2002, in Astrophysical Spectropolarimetry, ed. J. Trujillo-Bueno, F. Moreno-Insertis, & F. Sánchez, 303–354

Liu, Z., Deng, Y., & Ji, H. 2014, in IAU Symposium, Vol. 300, Nature of Prominences and their Role in Space Weather, ed. B. Schmieder, J.-M. Malherbe, & S. T. Wu, 349–354

Liu, Z., Deng, Y., Jin, Z., & Ji, H. 2012, in Society of Photo-Optical Instrumentation Engineers (SPIE) Conference Series, Vol. 8444, Ground-based and Airborne Telescopes IV, 844405

Liu, Z., Ji, H., Jin, Z., Lin, J., & Deng, Y. 2016, in Society of Photo-Optical Instrumentation Engineers (SPIE) Conference Series, Vol. 10012, Integrated Modeling of Complex Optomechanical Systems II, 1001204

McGuire, James P., J. & Chipman, R. A. 1990, Journal of the Optical Society of America A, 7, 1614

McGuire, James P., J. & Chipman, R. A. 1991, Journal of the Optical Society of America A, 8, 833

Rakic, A. D. 1995, Applied Optics, 34, 4755

Sanchez Almeida, J. & Martinez Pillet, V. 1992, Astronomy and Astrophysics, 260, 543

Stein, R. F. & Nordlund, Å. 2006, Astrophysical Journal, 642, 1246

van Weert, M. J. 1978, Journal of the Optical Society of America (1917-1983), 68, 1275